Gene Expression Changes Associated with Developing Resistance to Diffuse Intrinsic Pontine Glioma Treatments

Laura K. Harris *oesterei@msu.edu*
Institute for Cyber Enabled Research
Michigan State University
East Lansing, 48824, USA

Abstract

Background: Diffuse Intrinsic Pontine Glioma (DIPG) is a highly lethal pediatric brainstem tumor with limited treatment options. This work is the first to analyze differential gene expression across DIPG treatments to use a Gene Set Enrichment Analysis (GSEA)-based meta-analysis approach in identifying expression changes potentially contributing to the development of therapeutic resistance.

Methods: This work defines 14 gene signatures representing six individual and panobinostat combination treatments of DIPG patient-derived cell cultures. GSEA is used to define positive and negative panobinostat gene panels from GSEA-identified leading-edge genes using two panobinostat signatures. GSEA then is used to verify enrichment and leading-edge gene membership of panobinostat panels in two independent panobinostat signatures. Analysis is then extended to five individual and five panobinostat combination signatures. Genes most associated with treatment resistance are predicted by intersecting membership of GSEA-identified leading-edges across signatures.

Results: Significant enrichment is observed between panobinostat treatment identification signatures, from which the positive (25 genes) and negative (35 genes) panobinostat panels are defined. Non-random significant enrichment is observed between panobinostat panels and verification signatures, from which 17 over- and 30 under-expressed genes are shared across leading-edges. Considering other DIPG treatments individually and in combination with panobinostat, significant non-random enrichment is observed across treatment signatures, except 5-azacytidine, for the negative panobinostat panel. Six negative panobinostat panel genes, PHF19, ASCL1, KCNK2, EBP, ITPRIPL1, and LIN9, are found across treatment signature leading-edges regardless of treatment mechanism of action or combination with panobinostat.

Conclusion: This meta-analysis identifies gene expression changes associated with DIPG treatment. These changes may contribute to developing therapeutic resistance.

Keywords: Panobinostat, DIPG, GSEA, Meta-analysis, Gene Expression.

1. INTRODUCTION

Diffuse Intrinsic Pontine Glioma (DIPG) is a type of highly aggressive and often lethal pediatric brainstem tumor (Srikanthan et al., 2021). DIPG is rare, with ~250 new cases in the United States annually (Pellot & De Jesus, 2021), though DIPGs represent 80% of all childhood brain tumors (Srikanthan et al., 2021). Children diagnosed with DIPG have a median overall survival of ~11 months with a 2-year survival rate of only 10% (El-Khouly et al., 2019; Srikanthan et al., 2021), which is heartbreaking in a patient population where the median age at diagnosis is ~6.5 years (Srikanthan et al., 2021). Traditional oncology therapies, like radiotherapy and surgery, typically are unsuccessful or unsafe to attempt altogether due to tumor location (El-Khouly et al., 2019; Nagaraja et al., 2017). New therapeutic approaches for DIPG are desperately needed to improve prognosis for this patient population.

Recent years have brought a surge in research leading to a better understanding of the molecular mechanisms behind DIPG and the development of new therapeutic options (Nagaraja et al., 2017). Genomic studies showed that up to 85% of DIPG tumors exhibit a characteristic mutation of lysine 27 to methionine (K27M) in at least one of the genes encoding histone H3 (El-Khouly et al., 2019; Nagaraja et al., 2017; Pellot & De Jesus, 2021). The K27M mutation subsequently caused aberrant transcription in genes like the Polycomb repressive complex 2 (PRC2), resulting in global hypomethylation in all H3 variants and broad epigenetic dysregulation overall (Lin et al., 2019; Nagaraja et al., 2017). As of 2019, 90 clinical trials examining interventional therapies that target DIPG-related molecular mechanisms had been completed or were currently underway (Rechberger et al., 2020). Some potential therapies for DIPG that target epigenome changes, such as JMJD3 inhibitors like panobinostat and GSK-4 which target multi-histone deacetylase (HDAC) and demethylase, respectively, have shown promise in both laboratory and clinical studies (Srikanthan et al., 2021). While panobinostat has shown promise in restoring many gene expression changes associated with the K27M mutation in DIPG-derived cell lines, resistance to HDAC inhibition often develops forcing researchers to examine co-therapeutic options (Lin et al., 2019; Nagaraja et al., 2017). To compliment therapies directly targeting the epigenome, DIPG-derived epigenomic changes also have been targeted pharmacologically by leveraging the transcriptional dependencies of the tumor (Srikanthan et al., 2021). For example, transcriptional regulators targeting key activators of RNA polymerase II (RNAPII) transcription at active chromatin marks, like JQ1 (bromodomain BRD4 inhibitor) and THZ1 (cyclin-dependent kinase CDK7 inhibitor), showed promise in DIPG-derived cell lines when administered alone or in combination with panobinostat (Lin et al., 2019; Nagaraja et al., 2017; Srikanthan et al., 2021). Another example was the combination of panobinostat and marizomib (proteasome inhibitor) which also showed promise when treating an expanded panel of patient derived DIPG cell cultures and *in vivo* within orthotopic xenograft models (Borsuk et al., 2021; Lin et al., 2019). Combining panobinostat treatment with other epigenetic modifiers has shown potential also. For example, co-administration of panobinostat and CBL0137, which targets facilitates chromatin transcription (FACT), a chromatin remodeling complex involved in transcription, replication, and DNA repair, significantly prolongs the survival of DIPG orthografts bearing mice (Ehteda et al., 2021). Improved survival of mice injected with K27M cell lines were observed in mice treated with a combination of panobinostat with 5-azacytidine, a nucleoside analog which acts as a DNA demethylation agent, though researchers noted that additive toxicity of these compounds may limit their clinical potential as a combination therapy (Krug et al., 2019). Despite researchers having integrated insights from genomic, epigenomic and transcriptomic studies to better understand and target the tumorigenesis of DIPG, little success has been obtained in developing a cure (Chen et al., 2020; Rechberger et al., 2020).

A complete understanding of the molecular changes driving DIPG can assist in the development of new therapies. Several studies have been done to elucidate molecular changes associated with DIPG by examining gene expression changes in DIPG-patient derived cell cultures (Ehteda et al., 2021; Krug et al., 2019; Lin et al., 2019; Nagaraja et al., 2017). Some studies performed differential gene expression analysis, which was done on genes individually to identify genes of interest using pre-established statistical cut-off from methods like fold change (*e.g.*, fold change>2) and/or T-test p–value (*e.g.*, p-value<0.05). These studies found both JQ1 and panobinostat disrupted key regulators of nervous system development, including NTRK3, LINGO1, and ASCL1 (Nagaraja et al., 2017). Similarly, CBL0137 and panobinostat combination therapy also has been shown to downregulate key regulators of nervous system development, including LINGO1 and ASCL1, among other genes related to oligodendrocyte differentiation and lineage (Ehteda et al., 2021). In contrast, THZ1-treated cells showed preferential disruption of genes related to transcription and gene regulation such as SOX10 and HES5 (Nagaraja et al., 2017). Treatments involving 5-azacytidine has been shown to induce interferon type I signaling and expression of interferon stimulated genes (Krug et al., 2019). Treatments including marizomib have downregulated metabolism-related genes (Lin et al., 2019). Some studies expanded their gene expression analysis with subsequent pathway enrichment of resulting differential expression gene lists. For example, Nagaraja, et al., used hypergeometric test-based approaches (*e.g.*, Fisher's Exact Test) that utilized established gene sets from public

knowledgebases like Gene Ontology (GO) to interpret their resulting differential gene expression lists from JQ1, THZ1, and panobinostat treatments, and found enrichment of regulators of central nervous system differentiation, neurogenesis, and signal transduction (Nagaraja et al., 2017). However, hypergeometric test-based approaches are known to be limited because only genes that meet an established cut-off are considered (Subramanian et al., 2005). To overcome this limitation by considering all genes in an expression dataset, other studies utilized Gene Set Enrichment Analysis (GSEA) to calculate the enrichment of an established gene set from a public knowledgebase (*e.g.*, MSigDB) in a gene signature. Studies that performed GSEA using established cancer specific gene query sets and/or Cytoscape Enrichment Map visualizations found enrichment of Hallmark E2F targets genes in CBL0137 and panobinostat combination therapy (Ehteda et al., 2021). Further, oxidative-phosphorylation genes were consistently downregulated by combination panobinostat and marizomib treatment, and analysis of oxidative-phosphorylation leading edge genes demonstrated effects on the Complex I gene family (NADH:ubiquinone oxidoreductase subunits) and electron transport chain modulators like ATP5J2 (Lin et al., 2019). While these analysis extensions provide insight into molecular changes associated with DIPG treatments, these studies use GSEA for pathway enrichment, not gene identification. Application of GSEA to identify genes associated with DIPG itself or its treatments has yet to be performed, and such an analysis holds potential in uncovering molecular changes that adds depth to the current understanding of DIPG.

Previous work using a GSEA-based meta-analysis approach successfully identified known and novel genes associated with severe acute respiratory syndrome (SARS) infection through differential gene expression comparison between mRNA expression datasets (Park & Harris, 2021). Therefore, this paper differed from related work as it was the first to apply the same GSEA-based approach to analyze mRNA expression data of drug and mock treated DIPG-patient derived cell cultures by defining and comparing gene expression signatures (*i.e.*, gene lists ranked by differential expression). This paper started by using gene signatures to identify and verify gene expression changes associated with panobinostat treatment to elucidate molecular changes associated with the selective pressures driving resistance development. This paper further differed from related work as it was the first to apply a meta-analysis approach over publicly available independent datasets to examine similarities and differences in gene expression across a variety of DIPG treatments. Such an examination across DIPG treatments could provide insight into global therapeutic resistance mechanisms, something not previously examined. To do this, gene expression changes associated with panobinostat treatment were compared to changes resulting from other single and combination therapies to examine the therapy's potential to complement panobinostat treatment invoked changes. Gene expression changes identified across single and combination therapies may represent contributors to global therapeutic resistance and targeting these changes holds potential to increase treatment susceptibility.

2. METHODS

2.1 mRNA Expression Resources

To identify gene expression changes associated with treatment of DIPG cells, the Gene Expression Omnibus (GEO) repository (Clough & Barrett, 2016) was searched to find datasets for use in this study (Table 1). Since four independent series (GSE94259, GSE153441, GSE123278, and GSE117446) examined gene expression in panobinostat and mock treated *in vitro* cell cultures, our analysis started there. GSE94259 analyzed patient derived SU-DIPG-VI and SU-DIPG-XIII cell lines treated with DMSO (1%), panobinostat (0.1uM), JQ1 (1uM), THZ1 (0.1uM), or combination for 24 hours in growth media (Nagaraja et al., 2017). GSE153441 examined triplicate samples of HSJD-DIPG007 cells treated with DMSO, CBL0137 (0.6μM), panobinostat (20nM), and the combination of the two agents for 24 hours (Ehteda et al., 2021). GSE153441 samples were profiled on the Affymetrix Human Clariom D Assay (GPL28782). GSE123278 treated duplicate patient derived DIPG cell cultures (DIPG13, DIPG6, and R059) with DMSO, 50nM panobinostat, 20nM marizomib, or 50nM panobinostat and 20nM panobinostat for 16 hours (Lin et al., 2019). Further, GSE123278 contained DIPG13 samples treated with 100nM panobinostat

and 50nM marizomib (Combo High). GSE94259 and GSE123278 samples were profiled on Illumina NextSeq 500 for *Homo sapiens* (GPL18573). In GSE117446, two tumor derived cell lines (DIPGXIII and BT245) were treated with DMSO, panobinostat, 5-azacytidine (5-AZA), and a combination of both for each of the cell lines (Harutyunyan et al., 2020; Krug et al., 2019). GSE117446 samples used in this study were profiled on Illumina HiSeq 4000 for *Homo sapiens* (GPL20301).

Expression data provided by GEO for all datasets were z-scored normalized across all samples within the dataset regardless of treatment prior to use. Expression data was cleaned by removing GEO-provided probe identifiers where 1) all samples to be analyzed lacked data (*e.g.*, gene expression z-score of 0), or 2) duplicate identifiers were identified so only the identifier with the highest coefficient of variation were retained. All GEO-provided probes had an Ensemble gene ID and/or official gene symbol. If a dataset's GEO-provided platform contained both Ensemble gene IDs and gene symbols for a probe, the GEO-provided platform files to convert between these two prove identifiers were used. When a dataset's GEO-provided platform contained either Ensemble gene IDs or gene symbols for a probe, the Database for Annotation, Visualization, and Integrated Discovery (DAVID) v6.8 gene conversion tool was used (Huang da et al., 2009). Values provided in the Genes column in Table 1 reflect the number of normalized and cleaned genes used to define gene signatures for this study.

Dataset	Description	Platform	Probes	Genes
GSE94259	Cultures of DIPG13 and DIPG6 cells with 1% DMSO, 0.1μM panobinostat, 1μM JQ1, 0.1μM THZ1, combination panobinostat and JQ1, or combination panobinostat and THZ1 treatment for 24hrs	GPL18573	24606	24604
GSE153441	Cultures of HSJD-DIPG007 cells with DMSO, 20nM panobinostat, 0.6μM CBL0137, or combination panobinostat and CBL0137 treatment for 24hrs	GPL28782	46489	46489
GSE123278	Cultures of DIPG13, DIPG6, and R059 cells with DMSO, 50nM panobinostat, 20nM marizomib, or combination panobinostat and marizomib treatment for 16hrs	GPL18573	26839	23349
GSE117446	Cultures of six H3.3K27WT and seven H3.3K27M patient-derived cell lines with DMSO, 15nM panobinostat, 1.5μM 5-azacytidine, or combination panobinostat and 5-azacytidine treatment	GPL20301	60234	42281

TABLE 1: Datasets Utilized for this Study.

2.2 Defining Gene Signatures

To examine gene expression changes associated with DIPG treatment, differential gene expression was measured for samples of interest from each dataset using Welch's two-sample T-test score of cleaned and normalized values. Samples with the same treatment, regardless of strain or dosage, were combined to form one signature. The resulting list of genes and their T-test scores were used to define 14 gene signatures, which are gene lists ranked from high to low differential gene expression between treated versus control samples (Park & Harris, 2021). Signatures derived from the same dataset used the same control samples. The T-score range for each signature and the gene location where T-score becomes negative (*i.e.*, T-score=0) are found in Table 2.

Dataset	Group 1 (Number of Samples)	Group 2 (Number of Samples)	Gene Signature	Use	High	Low	Cross
GSE94259	panobinostat (4)	DMSO (4)	panovsDMSO	Identification	14.1	-11.7	12154
	JQ1 (4)	DMSO (4)	JQ1vsDMSO	Comparison	13.6	-12.2	8454
	THZ1 (4)	DMSO (4)	THZ1vsDMSO	Comparison	14.0	-14.1	1147
	JQ1 and panobinostat (4)	DMSO (4)	JQ1+panovsDMSO	Comparison	14.1	-13.5	8362
	THZ1 and panobinostat (4)	DMSO (4)	THZ1+panovsDMSO	Comparison	14.0	-14.1	1147
GSE153441	panobinostat (3)	DMSO (3)	panovsDMSO	Identification	12.2	-12.2	22148
	CBL0137 (3)	DMSO (3)	CBL0137vsDMSO	Comparison	12.2	-12.2	21819
	CBL0137 and panobinostat (3)	DMSO (3)	CBL0137+panovsDMSO	Comparison	12.2	-12.2	24334
GSE123278	panobinostat (6)	DMSO (6)	panovsDMSO	Verification	17.3	-17.2	12635
	marizomib (6)	DMSO (6)	marvsDMSO	Comparison	12.0	-17.0	10172
	marizomib and panobinostat (4)	DMSO (6)	mar+panovsDMSO	Comparison	18.4	-18.4	12258
GSE117446	panobinostat (5)	DMSO (6)	panovsDMSO	Verification	16.2	-15.7	26824
	5-azacytidine (5)	DMSO (6)	5AZAvsDMSO	Comparison	12.2	-12.2	29411
	5-azacytidine and panobinostat (5)	DMSO (6)	5AZA+panovsDMSO	Comparison	12.2	-12.2	28789

TABLE 2: Signatures Defined in this Study.

2.3 Identification of Genes Associated with Panobinostat Treatment

To identify gene expression changes associated with panobinostat treatment, two panobinostat gene panels were generated (Figure 1). To do this, 500 genes from the positive and negative tails from both the GSE94259-derived panovsmock and GSE153441-derived panovsmock gene signatures were selected and used to form four individual query gene sets. GSEA compared each query gene set to the both the entire GSE94259-derived panovsmock and GSE153441-derived panovsmock gene signatures (reference). Leading-edge (LE) genes from each analysis were examined and shared leading-edge genes were used to define two panobinostat gene panels, one panel per tail. Pathway enrichment analysis was performed on both panobinostat gene panels using DAVID.

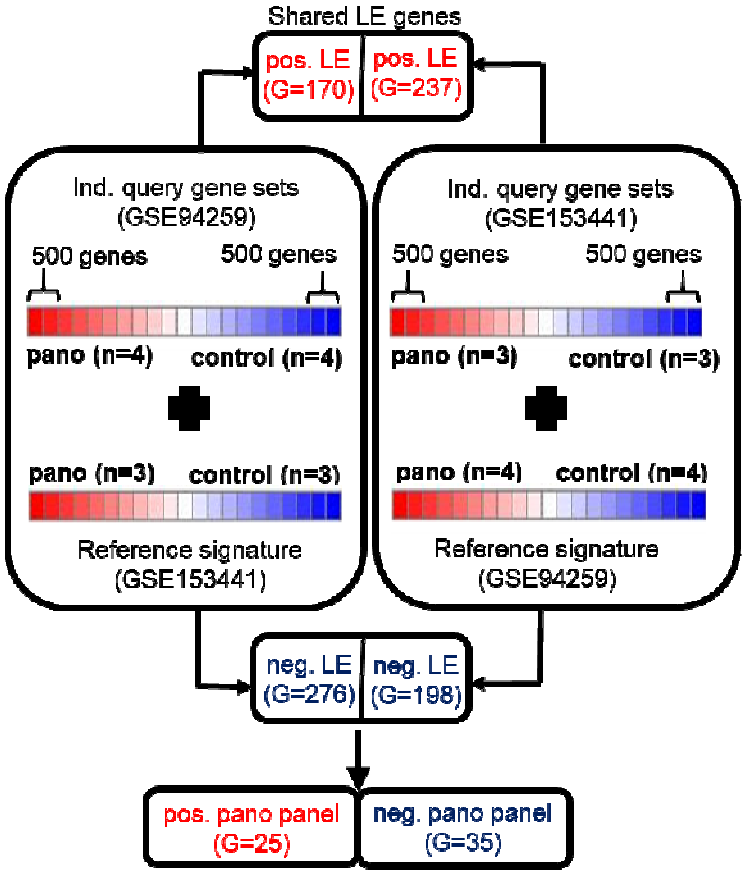

FIGURE 1: Schematic Overview of Gene Panel Identification.

2.4 Verification of Panobinostat Treatment Gene Panels

To verify the panobinostat gene panels, GSEA between panobinostat gene panels and GSE123278-derived and GSE117446-derived panovsmock signatures was performed. To assess if results generated from GSEA could be achieved randomly, 1000 gene panels consisting of 30-genes to match the average number of genes in the positive and negative panobinostat panels were randomly selected from the GPL28782 platform used to define the GSE153441 gene signatures used for gene identification for GSEA against GSE123278-derived and GSE117446-derived panovsmock signatures (references). These analyses generated a null distribution of NES to which were compared the NES achieved by panobinostat gene panels for each reference gene signature and count the number of equal or better NES to estimate significance (*i.e.*, null distribution p-value). Histogram data and associated graphs (*e.g.*, distribution curves and box and whiskers plot) were calculated using Excel.

2.5 Comparison of Panobinostat Treatment Gene Panels to Other DIPG Treatments

GSEA between panobinostat gene panels and gene signatures derived from samples of one of five treatments (JQ1, THZ1, CBL0137, Marizomib, or 5-azacytidine), either in single or combination therapy with pano, compared to control samples was performed to compare gene expression changes across DIPG treatments. Random modelling as previously described was used to assess if results generated from GSEA could be achieved randomly. Leading-edge genes from each statistically significant (GSEA p-value<0.05), non-random (null distribution p-value<0.05) GSEA were examined for common genes. T-scores from all 14 signatures defined in Table 2 for common genes identified were collected and converted into p-values for Stouffer's z-score analysis using the stats.combine_pvalues command from the scipy package in Python 3.8.

3. RESULTS

3.1 Gene Signature Approach Identified Gene Expression Changes Associated with Panobinostat Treatment of DIPG Cells *in vitro*

GSE153441-derived and GSE94259-derived panovsmock gene signatures were defined to identify genes associated with response to panobinostat treatment of human DIPG cells (Table 2). From both these two panovsmock identification signatures, two gene sets were generated containing the 500 most differentially expressed genes from the positive and negative tails of each signature, capturing maximum coverage of the signature that was allowable by GSEA (Subramanian et al., 2005). The T-score of selected query genes from the GSE94259-derived panovsmock signature were >5.6 and <-4.9 and >16.6 and <-16.8 from the GSE153441-derived panovsmock signature for positive and negative tails, respectively. To assess similarity between these two signatures, enrichment was first calculated using GSEA between GSE94259-derived panovsmock positive or negative tail gene sets (individual queries) and the GSE153441-derived panovsmock (reference) and achieved NES=2.86 and NES=-2.19 for positive and negative tail query gene sets, respectively, both with a GSEA p-value<0.001. Similar findings were observed when GSEA calculated enrichment between GSE153441-derived panovsmock positive (NES=1.71) and negative (NES=-2.88) tail gene sets and the GSE94259-derived panovsmock (p-value<0.001). Identified leading-edge genes from these GSEA are listed in Supplemental Material STables 1 and 2. Separate positive and negative panobinostat gene panels from the 25 and 35 shared leading-edge genes identified were defined (Tables 3 and 4, respectively), representing over- and under-expressed genes associated with panobinostat treatment.

No genes in the positive panobinostat panel were mentioned in the published reports for GSE94259 and GSE153441, though some panel genes like amidohydrolase domain containing 2 (AMDHD2) have reported connections with panobinostat treatment in the literature (Choi et al., 2019). In the negative DIPG gene panel, two genes, v-myc avian myelocytomatosis viral oncogene homolog (MYC) and achaete-scute family bHLH transcription factor 1 (ASCL1), were found to have previous associations with panobinostat treatment of DIPG cells (Ehteda et al., 2021; Nagaraja et al., 2017). Taken together, this demonstrated the detection ability of using a GSEA-based approach to gene identification. The rest of the genes in the negative panobinostat panel had no prior association with panobinostat treatment of DIPG cells from the published reports for GSE94259 and GSE153441. It can be speculated that genes lacking previously reported associations with panobinostat treatment that were identified here also are associated with panobinostat treatment of DIPG cell cultures. Therefore, this paper is the first to report the association of these gene expression changes with panobinostat treatment.

To expand our analysis, the cellular roles of DIPG panel genes were examined using DAVID to calculate enrichment between each DIPG panel and pathways in popular knowledgebases. It was noticed that, when compared to other databases, the GO BP database returned the most significantly enriched pathways (data not shown), hence this discussion was concentrated on GO-BP data to prevent confusion caused by overlapping pathway and gene inclusion differences across multiple knowledgebases. DAVID identified four significant GO-BP pathways (EASE score

p-value<0.05) from the positive DIPG panel and six significant pathways from the negative DIPG panel (Supplemental Material STable 3). Some significantly enriched pathways have experimentally established associations with panobinostat treatment of DIPG, such as transferrin transport pathway (GO:0033572, p-value=0.04) and Notch signaling pathway (GO:0007219, p−value=0.018), demonstrating the ability of our gene signature approach to detect pathways associated with panobinostat treatment (Taylor et al., 2015; Tu et al., 2020). Other identified pathways, such as negative regulation of transcription from RNA polymerase II promoter (GO:0000122, p-value=0.009), have no prior associations to panobinostat treatment. Therefore, it can be speculated that pathways without prior association to DIPG identified here also were involved in DIPG, and that this paper is the first to report the association of these pathway activity changes with panobinostat treatment.

Ensembl ID	Symbol	Description
ENSG00000154639	CXADR	coxsackie virus and adenovirus receptor
ENSG00000169116	PARM1	prostate androgen-regulated mucin-like protein 1
ENSG00000148180	GSN	gelsolin
ENSG00000197948	FCHSD1	FCH and double SH3 domains 1
ENSG00000147416	ATP6V1B2	ATPase H+ transporting V1 subunit B2
ENSG00000197943	PLCG2	phospholipase C gamma 2
ENSG00000162066	AMDHD2	amidohydrolase domain containing 2
ENSG00000135525	MAP7	microtubule associated protein 7
ENSG00000130517	PGPEP1	pyroglutamyl-peptidase I
ENSG00000164953	TMEM67	transmembrane protein 67
ENSG00000136960	ENPP2	ectonucleotide pyrophosphatase/phosphodiesterase 2
ENSG00000085552	IGSF9	immunoglobulin superfamily member 9
ENSG00000130158	DOCK6	dedicator of cytokinesis 6
ENSG00000197892	KIF13B	kinesin family member 13B
ENSG00000134996	OSTF1	osteoclast stimulating factor 1
ENSG00000008056	SYN1	synapsin I
ENSG00000075223	SEMA3C	semaphorin 3C
ENSG00000165959	CLMN	calmin
ENSG00000076641	PAG1	phosphoprotein membrane anchor with glycosphingolipid microdomains 1
ENSG00000139182	clstn3	calsyntenin 3
ENSG00000155097	ATP6V1C1	ATPase H+ transporting V1 subunit C1
ENSG00000156869	FRRS1	ferric chelate reductase 1
ENSG00000122735	DNAI1	dynein axonemal intermediate chain 1
ENSG00000169432	SCN9A	sodium voltage-gated channel alpha subunit 9
ENSG00000150627	WDR17	WD repeat domain 17

TABLE 3: Positive Panobinostat Gene Panel Defined in this Study.

Ensembl ID	Symbol	Description
ENSG00000119403	PHF19	PHD finger protein 19
ENSG00000133393	FOPNL	FGFR1OP N-terminal like
ENSG00000136997	MYC	v-myc avian myelocytomatosis viral oncogene homolog
ENSG00000119865	CNRIP1	cannabinoid receptor interacting protein 1
ENSG00000165449	SLC16A9	solute carrier family 16 member 9
ENSG00000162733	DDR2	discoidin domain receptor tyrosine kinase 2
ENSG00000170365	SMAD1	SMAD family member 1
ENSG00000139352	ASCL1	achaete-scute family bHLH transcription factor 1
ENSG00000162623	TYW3	tRNA-yW synthesizing protein 3 homolog
ENSG00000082482	KCNK2	potassium two pore domain channel subfamily K member 2
ENSG00000105483	CARD8	caspase recruitment domain family member 8
ENSG00000165458	INPPL1	inositol polyphosphate phosphatase like 1
ENSG00000179981	TSHZ1	teashirt zinc finger homeobox 1
ENSG00000148840	PPRC1	peroxisome proliferator-activated receptor gamma, coactivator-related 1
ENSG00000135097	MSI1	musashi RNA binding protein 1
ENSG00000106991	ENG	endoglin
ENSG00000112667	DNPH1	2'-deoxynucleoside 5'-phosphate N-hydrolase 1
ENSG00000169857	AVEN	apoptosis and caspase activation inhibitor
ENSG00000031081	ARHGAP31	Rho GTPase activating protein 31
ENSG00000035681	NSMAF	neutral sphingomyelinase activation associated factor
ENSG00000107130	NCS1	neuronal calcium sensor 1
ENSG00000147155	EBP	emopamil binding protein
ENSG00000120800	UTP20	UTP20, small subunit processome component
ENSG00000143222	UFC1	ubiquitin-fold modifier conjugating enzyme 1
ENSG00000198885	ITPRIPL1	inositol 1,4,5-trisphosphate receptor interacting protein-like 1
ENSG00000184489	PTP4A3	protein tyrosine phosphatase type IVA, member 3
ENSG00000183814	LIN9	lin-9 DREAM MuvB core complex component
ENSG00000076770	MBNL3	muscleblind like splicing regulator 3
ENSG00000109320	NFKB1	nuclear factor kappa B subunit 1
ENSG00000018699	TTC27	tetratricopeptide repeat domain 27
ENSG00000143436	MRPL9	mitochondrial ribosomal protein L9
ENSG00000116157	GPX7	glutathione peroxidase 7
ENSG00000063601	MTMR1	myotubularin related protein 1
ENSG00000073849	st6gal1	ST6 beta-galactoside alpha-2,6-sialyltransferase 1
ENSG00000047230	CTPS2	CTP synthase 2

TABLE 4: Negative Panobinostat Gene Panel Defined in this Study.

3.2 Enrichment of Panobinostat Gene Panels and Specific Panobinostat Panel Genes Verified in Independent Datasets

To verify our panobinostat gene panels, GSEA was used to calculate enrichment between our panobinostat panels (individual queries) and two verification gene signatures (individual references): GSE117446-derived panovsmock and GSE123278-derived panovsmock (Table 2). Significant similarity between positive and negative panobinostat panels and GSE117446-derived panovsmock (NES=2.55 for the positive panobinostat panel, Figure 2A, and NES=-3.04 for the negative panobinostat panel, Figure 2B, both GSEA p-value<0.001) was found. To determine how likely the NES achieved for panobinostat panels would be achieved by random chance, 1000 randomly selected 30-gene panels were generated from the GSE153441-derived panovsmock gene signature to match the average size and potential composition of our panobinostat panels. GSEA was then repeated using these randomly generated gene panels (individual queries) and

the GSE117446-derived panovsmock (reference) to generate a null distribution of NES achieved via random chance. From this, random NES ranged from 1.80 to -1.66 was found (Figure 2C), illustrating that NES achieved by our panobinostat panels are non-random (null distribution p-value<0.001). For GSE123278-derived panovsmock, similarity was again observed with positive and negative panobinostat panels (NES=2.32 for the positive panel, Figure 2D, and NES=-2.72 for the negative panel, Figure 2E, both GSEA p-value<0.001). Random NES ranged from 1.99 to -1.82 (Figure 2F), showing achieved results were non-random (both panel null p-value<0.001). Taken together, these results demonstrate that the enrichment achieved from our panobinostat panels was true.

To determine which of our panobinostat panel genes were verified across all signatures, leading-edge genes identified by GSEA for each verification signature were examined. Leading-edge genes for GSE123278-derived and GSE117446-derived panovsmock signatures are listed in Supplemental Material STables 4 and 5, respectively. Seventeen genes from the positive panobinostat panel and 30 genes from the negative panobinostat panel were shared between verification signatures. ASCL1 was among verified genes with prior reported associations to panobinostat treatment (Ehteda et al., 2021; Nagaraja et al., 2017), though it was not mentioned in the published reports from GSE123278 and GSE117446 (Krug et al., 2019; Lin et al., 2019). These data together verified our shared leading-edge genes were associated with panobinostat treatment in human DIPG cultures and support the hypothesis that identified genes without previously reported associations also were associated with panobinostat treatment in human DIPG cultures. Verified gene expression changes associated with panobinostat treatment may have more potential as future DIPG therapeutic targets compared to genes identified earlier that could not be verified, despite lack of previously reported associations.

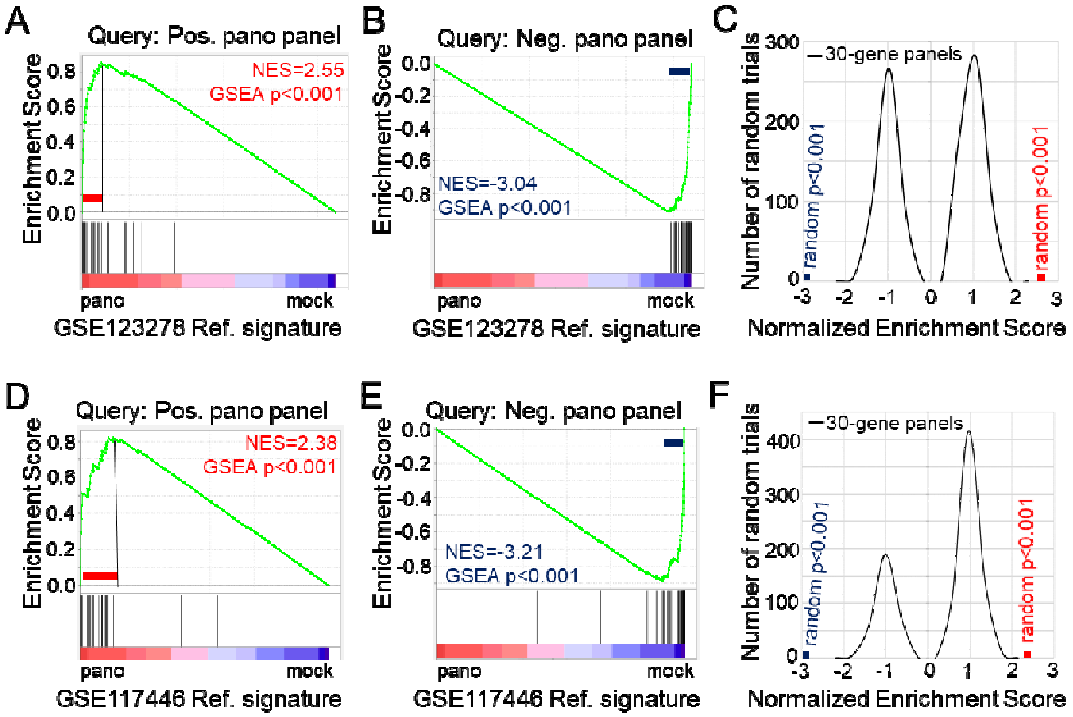

FIGURE 2: Schematic Overview of Gene Panel Identification.

3.3 Non-random Enrichment of Panobinostat Gene Panels Found in Other DIPG Treatments

To expand this study, gene expression changes associated with panobinostat were compared to changes observed in other DIPG treatments included in GEO Series previously used to examine

panobinostat treatment. The following 10 signatures were examined: JQ1vsDMSO, THZ1vsDMSO, JQ1+panovsDMSO, THZ1+panovsDMSO, CBL0137vsDMSO, CBL0137+panovsDMSO, marvsDMSO, mar+panovsDMSO, 5AZAvsDMSO, and 5AZA+panovsDMSO (Table 2). Since JQ1 and THZ1 impact transcription factors, BRD4 and CDK7, respectively, that work together as part of the RNA polymerase II (RNAPII) complex to transcribe DIPG oncogenes and panobinostat inhibits histone deacetylation which alters RNAPII access to DIPG oncogenes for transcription, similarities in differential gene expression between the verified panobinostat panels and the four GSE94259-derived signatures was expected (Nagaraja et al., 2017). Significant (GSEA p-values<0.013), non-random (null distribution p-values<0.004) enrichment between both positive and negative panobinostat panels in JQ1vsDMSO and JQ1+panovsDMSO signatures were found (Figure 3), indicating that JQ1 may share mechanisms with panobinostat. For both THZ1vsDMSO and THZ1+panovsDMSO signatures, only the negative panobinostat panel achieved significant, non-random enrichment (Figure 3). Interestingly, the positive panobinostat panel for both THZ1vsDMSO and THZ1+panovsDMSO signatures had a negative NES (Figure 3) and these signatures were skewed to have substantially more genes with a negative T-score (Table 2), leading to the conclusion that THZ1 may function to reduce cell proliferation by inhibiting general gene expression. Similarities between differential expression based on CBL0137 and panobinostat treatment were expected also since both therapies synergistically inhibit the Rb/E2F1 pathway (Ehteda et al., 2021). Significant (GSEA p-values<0.001), non-random (null distribution p-values<0.001) enrichment between both positive and negative panobinostat panels in CBL0137vsDMSO and CBL0137+panovsDMSO signatures were found (Figure 3), supporting previous findings that CBL0137 and panobinostat share some mechanisms. Though panobinostat and marizomib (a proteasome inhibitor) have substantially different mechanisms of action, reports of their synergistic action to combat DIPG lead to the hypothesis that these therapies may share some mechanisms. Significant (GSEA p-values<0.008), non-random (null distribution p-values<0.001) enrichment between both positive and negative panobinostat panels in marvsDMSO and mar+panovsDMSO signatures were found (Figure 3), indicating that marizomib may share mechanisms with panobinostat. Since 5-azacytidine is a gene demethylating agent that also works to regulate gene expression through global epigenetic changes, similarities in gene expression changes between 5-azacytidine and panobinostat were expected (Jubierre et al., 2018). However, for 5-azacytidine, both panobinostat gene panels were non-randomly (null distribution p-values<0.001), enriched in the 5AZA+panovsDMSO signature, but neither panobinostat panel achieved significant enrichment (GSEA p-values>0.078) in the 5AZAvsDMSO signature (Figure 3). This finding suggests that 5-azacytidine does not share mechanisms to combat DIPG with panobinostat, but that effects of panobinostat treatment is detectable in combination therapy using a gene signature approach.

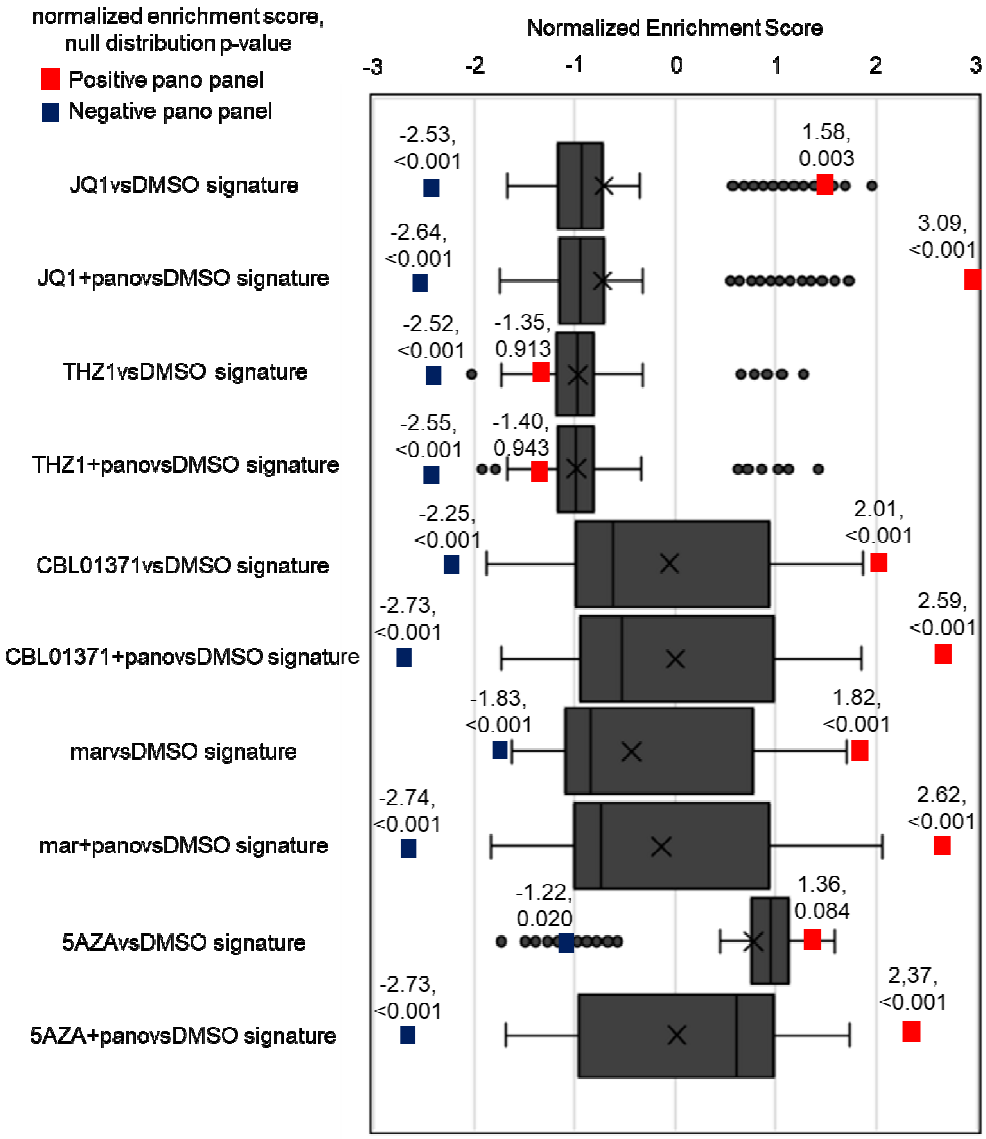

FIGURE 3: Enrichment of Panobinostat Gene Panels and Random Models Across DIPG Treatments.

3.4 Leading-edge Genes Found Across DIPG Treatments

Finally, leading-edge genes from each GSEA across DIPG treatments were examined to identify genes of potential interest. Supplemental Material STables 6 through 15 contains leading-edge genes from GSEA with each panobinostat gene panel (Tables 3 and 4) across 10 comparison gene signatures (Table 2). Leading-edge genes from each GSEA across all signatures, except 5AZAvsDMSO and the positive panobinostat panel for THZ1vsDMSO and THZ1+panovsDMSO because these GSEA failed to achieve statistical significance (GSEA p-value>0.05) and/or non-randomness (null distribution>0.05), were collected to see which genes were most associated with treatment of DIPG cells. Two positive panobinostat panel genes commonly found across DIPG treatments, a prostate androgen-regulated mucin-like protein 1 (PARM1) and a semaphorin 3C (SEMA3C). Neither PARM1 or SEMA3C were associated with DIPG or its treatment, though PARM1 was reported as upregulated during Trichostatin A, a HDAC class I and II inhibitor, treatment of SK-MEL-3 Melanoma Cells (Mazzio & Soliman, 2018), and SEMA3C has reported connections to cervical and other cancer (Liu et al., 2019; Peacock et al., 2018). There were eight negative panobinostat panel genes in common across DIPG treatments, a PHD finger protein 19

(PHF19), achaete-scute family bHLH transcription factor 1 (ASCL1), potassium two pore domain channel subfamily K member 2 (KCNK2), emopamil binding protein (EBP), inositol 1,4,5-trisphosphate receptor interacting protein-like 1 (ITPRIPL1), lin-9 DREAM MuvB core complex component (LIN9), glutathione peroxidase 7 (GPX7), and CTP synthase 2 (CTPS2). All common negative panobinostat panel genes except GPX7 and CTPS2 were included in the leading-edge for 5AZAvsDMSO (Supplemental Material STable 14). There was no connection between LIN9, KCNK2, EBP, or ITPRIPL1 and DIPG or its treatment reported, though there were reports connecting DIPG or its treatment to PHF19 and ASCL1. Over-expressed PHF19 was associated with poor prognosis in glioblastoma patients and PHF19 knockdown models showed a clear increase in doxorubicin-induced apoptosis (Deng et al., 2018). Also, PHF19 inhibition has shown promise as a therapeutic target for multiple myeloma (Schinke et al., 2021), though attempts at PHF19 inhibition of DIPG have not been reported. Treatment with JQ1 alone, panobinostat alone, or CBL0137 and panobinostat in combination have been shown to disrupt ASCL1 activity (Ehteda et al., 2021; Nagaraja et al., 2017).

To rank shared leading-edge genes, Stouffer's z-score was used. Z-scores for negative panobinostat panel genes were higher than for positive panobinostat panel genes (Figure 4), complementing the strength of negative panobinostat panel enrichment observed previously (Figure 3). Of negative panobinostat panel genes, the potassium two pore domain channel subfamily K member 2 (KCNK2) and inositol 1,4,5-trisphosphate receptor interacting protein-like 1 (ITPRIPL1) had the highest z-score (Figure 4). From these results, it could be hypothesized that top scoring genes identified here are more likely to play a role in the treatment of DIPG cells despite this being the first report of association between these genes and DIPG or its treatment.

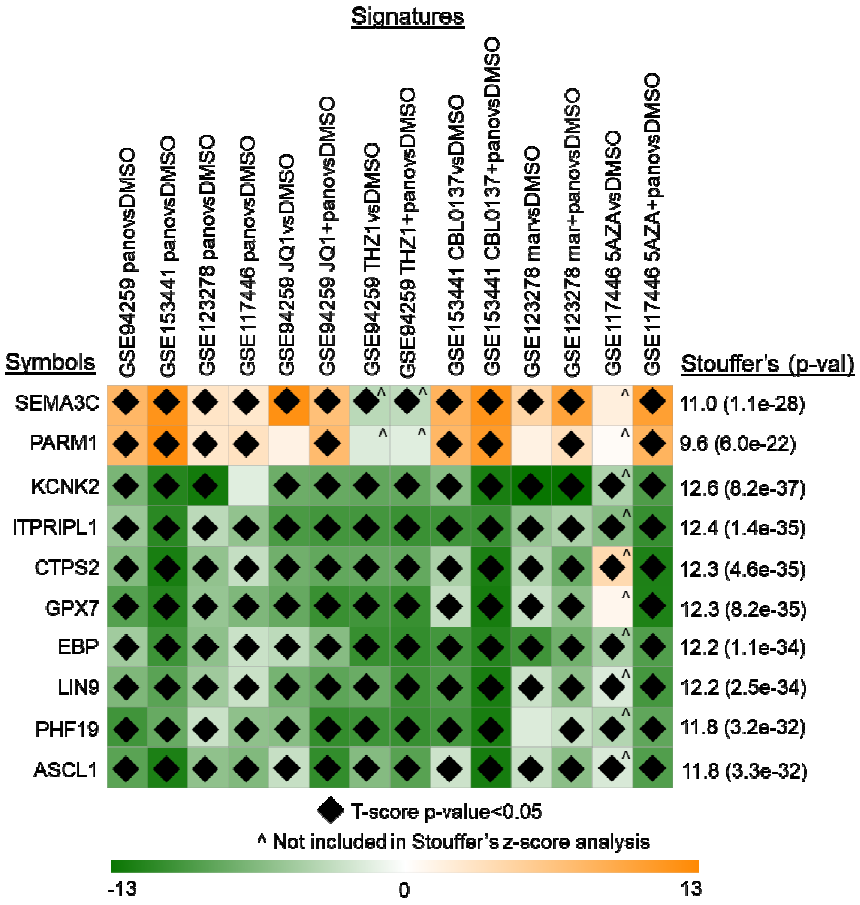

FIGURE 4: Heat Map of LE Genes Shared Across DIPG Treatments.

4. DISCUSSION

DIPG remains a highly aggressive childhood brainstem tumor with little hope for a favorable prognosis. While efforts have gone into developing effective therapies for DIPG patients, treatment resistance is a major limitation, due in part to an incomplete understanding of the molecular changes behind resistance development. Identification of differentially expressed genes associated with treatment itself can contribute to the overall understanding of the molecular changes that drive resistance development. This improved understanding can potentially contribute to the development of new therapeutic options to improve the prognosis for DIPG patients. This work conducted a meta-analysis of gene expression signatures generated from mRNA expression data across panobinostat and five other DIPG treatments, both individually and in combination with pano, to identify differentially expressed genes associated with DIPG treatment. Genes that change in response to treatment may contribute to developing treatment resistance long-term.

Among genes identified by this work, six under-expressed gene candidates, PHF19, ASCL1, LIN9, KCNK2, EBP, and ITPRIPL1, stood out consistently across treatments. PHF19 was one of the Polycomb Repressive Complex 2 (PRC2) ancillary subunits. Reports existed associating the common H3K27M mutation in DIPG to PRC2 inhibition though the exact involvement of PHF19 remains unclear (Bracken et al., 2019; Jain et al., 2019; Lin et al., 2019). ASCL1 was a member of the adrenergic neuroblastoma core regulatory circuitry (Wang et al., 2019). ASCL1 has been shown to regulate cell cycle genes in glioma mouse models, and ASCL1 overexpression has been associated with DIPG cell fitness and tumorigenicity (Fortin et al., 2020; J. Wang et al., 2021). LIN9 was a critical mitosis regulator with connections to breast cancer. LIN9 was suppressed by JQ1 in breast cancer cells and may have potential as a Bromodomain and Extraterminal inhibitor (BETi) response prediction marker clinically (Sahni & Keri, 2018). The association between LIN9 and DIPG was not established. Further, the association between DIPG and KCNK2, EBP, and ITPRIPL1 were not established either. KCNK2 (also known as TREK-1) is a member of the two-pore-domain K+ channel family responsible for maintaining neuronal resting membrane potential and the duration of action potentials. Reduced expression of KCNK2 was reported in liver cancer with reports of KCNK2 overexpression in prostate, epithelial ovarian cancer, and other cancer types (Li et al., 2019). EBP was the 3-β-hydroxysteroid-δ(8), δ(7)-isomerase in the postsqualene cholesterol biosynthetic pathway with associations to breast, prostate, and colorectal cancers (Ershov et al., 2021; Long et al., 2019; Theodoropoulos et al., 2020). ITPRIPL1 was an inositol 1,4,5-trisphosphate receptor interacting protein shown recently to have aberrant methylation in breast cancer patients but not in lung, uterine, ovarian, gastric, esophagus, pancreatic, liver, or colorectal cancers via bioinformatic analysis (S. C. Wang et al., 2021). Taken together, these results suggested that the GSEA-based meta-analysis approach used here was successful in identifying cancer-related genes with and without DIPG associations.

This work had observable gene detection limitations that may have biological implications. For example, gene expression changes commonly associated with DIPG treatment in genes like PRC2, TP53, BRD4, EGFR, and PDGFRA were not found in this study (Ehteda et al., 2021; Krug et al., 2019; Lapin et al., 2017; Lin et al., 2019; Nagaraja et al., 2017; Srikanthan et al., 2021). In the cases of PRC2 and TP53, these genes were not included in the platform of one or more datasets used in this work. Platform variations, both in gene inclusion and primer nucleotide sequence, can substantially impact results generated from this, or any, bioinformatics analysis. While BRD4, EGFR, and PDGFRA were included in the GSE94259 identification dataset, their T-scores were insufficient to make the 500 gene cut-off required of GSEA to maintain statistical accuracy. This is an inherent limitation with the use of GSEA, which can only be overcome by switching to a non-GSEA based method. However, if the desired outcome is a prioritized list of potential gene candidates for further laboratory or clinical examination, the GSEA-based approach used here suffices.

A lack of direct experimental or clinical evidence substantially limited the conclusions drawn from this purely bioinformatics work. Follow-up experiments using laboratory techniques, such as Western blotting or qRT-PCR, to confirm top gene candidate predictions would support these

conclusions drawn exclusively from mRNA expression data. Further, due to their public availability, datasets selected for this work examined short treatment durations ($\leq$24 hours) in human DIPG cultures only. Further analysis examining gene expression data from cell cultures undergoing longer treatment durations that more closely mimic clinical cases is needed. Further, gene expression data directly from DIPG patients would be of particular interest to further explore the results generated here. Such an examination of gene expression data from treated and untreated human DIPG samples would be limited due to challenges acquiring samples from tumor location.

5. CONCLUSION

This work is the first to examine mRNA expression data to predict genes potentially involved in developing resistance to DIPG treatments through examining gene signatures using a GSEA-based meta-analysis approach. Six under-expressed genes, PHF19, ASCL1, KCNK2, EBP, ITPRIPL1, and LIN9, were identified as being most associated with DIPG treatment regardless of mechanism of action or combination with panobinostat. This work demonstrated the usefulness of a computational meta-analysis approach used previously to detect genes associated with SARS infection in identifying genes associated with DIPG treatment through application on mRNA expression data from DIPG therapeutic and DMSO treated cell cultures. Experimental biologists can confirm these computational predictions immediately through the generation and subsequent examination of knock-out (*i.e.*, single selected gene mutation resulting in loss of function) cell lines derived from the DIPG cultures used to generate the mRNA expression data used in this study. Researchers then can develop compounds to target genes with observed therapeutic sensitivity changes experimentally. Such efforts could lead to the successful development of co-therapies to raise efficacy of current DIPG therapeutics long-term, ultimately improving how clinicians treat DIPG patients.

6. ACKNOWLEDGEMENTS

Thanks to Rutvi Vaja for assisting with topic selection, preliminary analysis, and manuscript writing. Thanks to Terri Pulice for the graphic design assistance and Anton Oestereicher for the financial support.

7. REFERENCES

Borsuk, R., Zhou, L., Chang, W.-i., Zhang, Y., Prabhu, V., Allen, J., Tapinos, N., Lulla, R., & El-Deiry, W. (2021). HGG-42. Pediatric H3K27M Mutant Diffuse Intrinsic Pontine Glioma (DIPG) Shows Robust Response to Imipridone based combination Therapy. *Neuro-Oncology*, *23*(Supplement_1), i26-i26. https://doi.org/10.1093/neuonc/noab090.106.

Bracken, A. P., Brien, G. L., & Verrijzer, C. P. (2019). Dangerous liaisons: interplay between SWI/SNF, NuRD, and Polycomb in chromatin regulation and cancer. *Genes Dev*, *33*(15-16), 936-959. https://doi.org/10.1101/gad.326066.119.

Chen, L. H., Pan, C., Diplas, B. H., Xu, C., Hansen, L. J., Wu, Y., Chen, X., Geng, Y., Sun, T., Sun, Y., Zhang, P., Wu, Z., Zhang, J., Li, D., Zhang, Y., Wu, W., Wang, Y., Li, G., Yang, J., . . . Zhang, L. (2020). The integrated genomic and epigenomic landscape of brainstem glioma. *Nat Commun*, *11*(1), 3077. https://doi.org/10.1038/s41467-020-16682-y.

Choi, S. A., Lee, C., Kwak, P. A., Park, C. K., Wang, K. C., Phi, J. H., Lee, J. Y., Chong, S., & Kim, S. K. (2019). Histone deacetylase inhibitor panobinostat potentiates the anti-cancer effects of mesenchymal stem cell-based sTRAIL gene therapy against malignant glioma. *Cancer Lett*, *442*, 161-169. https://doi.org/10.1016/j.canlet.2018.10.012.

Clough, E., & Barrett, T. (2016). The Gene Expression Omnibus Database. *Methods Mol Biol*, *1418*, 93-110. https://doi.org/10.1007/978-1-4939-3578-9_5.

Deng, Q., Hou, J., Feng, L., Lv, A., Ke, X., Liang, H., Wang, F., Zhang, K., Chen, K., & Cui, H. (2018). PHF19 promotes the proliferation, migration, and chemosensitivity of glioblastoma to doxorubicin through modulation of the SIAH1/beta-catenin axis. *Cell Death Dis*, *9*(11), 1049. https://doi.org/10.1038/s41419-018-1082-z.

Ehteda, A., Simon, S., Franshaw, L., Giorgi, F. M., Liu, J., Joshi, S., Rouaen, J. R. C., Pang, C. N. I., Pandher, R., Mayoh, C., Tang, Y., Khan, A., Ung, C., Tolhurst, O., Kankean, A., Hayden, E., Lehmann, R., Shen, S., Gopalakrishnan, A., . . . Ziegler, D. S. (2021). Dual targeting of the epigenome via FACT complex and histone deacetylase is a potent treatment strategy for DIPG. *Cell Rep*, *35*(2), 108994. https://doi.org/10.1016/j.celrep.2021.108994.

El-Khouly, F. E., Veldhuijzen van Zanten, S. E. M., Santa-Maria Lopez, V., Hendrikse, N. H., Kaspers, G. J. L., Loizos, G., Sumerauer, D., Nysom, K., Pruunsild, K., Pentikainen, V., Thorarinsdottir, H. K., Rutkauskiene, G., Calvagna, V., Drogosiewicz, M., Dragomir, M., Deak, L., Kitanovski, L., von Bueren, A. O., Kebudi, R., . . . van Vuurden, D. G. (2019). Diagnostics and treatment of diffuse intrinsic pontine glioma: where do we stand? *J Neurooncol*, *145*(1), 177-184. https://doi.org/10.1007/s11060-019-03287-9.

Ershov, P., Kaluzhskiy, L., Mezentsev, Y., Yablokov, E., Gnedenko, O., & Ivanov, A. (2021). Enzymes in the Cholesterol Synthesis Pathway: Interactomics in the Cancer Context. *Biomedicines*, *9*(8). https://doi.org/10.3390/biomedicines9080895.

Fortin, J., Tian, R., Zarrabi, I., Hill, G., Williams, E., Sanchez-Duffhues, G., Thorikay, M., Ramachandran, P., Siddaway, R., Wong, J. F., Wu, A., Apuzzo, L. N., Haight, J., You-Ten, A., Snow, B. E., Wakeham, A., Goldhamer, D. J., Schramek, D., Bullock, A. N., . . . Mak, T. W. (2020). Mutant ACVR1 Arrests Glial Cell Differentiation to Drive Tumorigenesis in Pediatric Gliomas. *Cancer Cell*, *37*(3), 308-323 e312. https://doi.org/10.1016/j.ccell.2020.02.002.

Harutyunyan, A. S., Chen, H., Lu, T., Horth, C., Nikbakht, H., Krug, B., Russo, C., Bareke, E., Marchione, D. M., Coradin, M., Garcia, B. A., Jabado, N., & Majewski, J. (2020). H3K27M in Gliomas Causes a One-Step Decrease in H3K27 Methylation and Reduced Spreading within the Constraints of H3K36 Methylation. *Cell Rep*, *33*(7), 108390. https://doi.org/10.1016/j.celrep.2020.108390.

Huang da, W., Sherman, B. T., & Lempicki, R. A. (2009). Systematic and integrative analysis of large gene lists using DAVID bioinformatics resources. *Nat Protoc*, *4*(1), 44-57. https://doi.org/10.1038/nprot.2008.211.

Jain, S. U., Do, T. J., Lund, P. J., Rashoff, A. Q., Diehl, K. L., Cieslik, M., Bajic, A., Juretic, N., Deshmukh, S., Venneti, S., Muir, T. W., Garcia, B. A., Jabado, N., & Lewis, P. W. (2019). PFA ependymoma-associated protein EZHIP inhibits PRC2 activity through a H3 K27M-like mechanism. *Nat Commun*, *10*(1), 2146. https://doi.org/10.1038/s41467-019-09981-6.

Jubierre, L., Jimenez, C., Rovira, E., Soriano, A., Sabado, C., Gros, L., Llort, A., Hladun, R., Roma, J., Toledo, J. S., Gallego, S., & Segura, M. F. (2018). Targeting of epigenetic regulators in neuroblastoma. *Exp Mol Med*, *50*(4), 1-12. https://doi.org/10.1038/s12276-018-0077-2.

Krug, B., De Jay, N., Harutyunyan, A. S., Deshmukh, S., Marchione, D. M., Guilhamon, P., Bertrand, K. C., Mikael, L. G., McConechy, M. K., Chen, C. C. L., Khazaei, S., Koncar, R. F., Agnihotri, S., Faury, D., Ellezam, B., Weil, A. G., Ursini-Siegel, J., De Carvalho, D. D., Dirks, P. B., . . . Mack, S. C. (2019). Pervasive H3K27 Acetylation Leads to ERV Expression and a Therapeutic Vulnerability in H3K27M Gliomas. *Cancer Cell*, *35*(5), 782-797 e788. https://doi.org/10.1016/j.ccell.2019.04.004.

Lapin, D. H., Tsoli, M., & Ziegler, D. S. (2017). Genomic Insights into Diffuse Intrinsic Pontine Glioma. *Front Oncol*, *7*, 57. https://doi.org/10.3389/fonc.2017.00057.

Li, W. C., Xiong, Z. Y., Huang, P. Z., Liao, Y. J., Li, Q. X., Yao, Z. C., Liao, Y. D., Xu, S. L., Zhou, H., Wang, Q. L., Huang, H., Zhang, P., Lin, J. Z., Liu, B., Ren, J., & Hu, K. P. (2019). KCNK levels are prognostic and diagnostic markers for hepatocellular carcinoma. *Aging (Albany NY)*, *11*(19), 8169-8182. https://doi.org/10.18632/aging.102311.

Lin, G. L., Wilson, K. M., Ceribelli, M., Stanton, B. Z., Woo, P. J., Kreimer, S., Qin, E. Y., Zhang, X., Lennon, J., Nagaraja, S., Morris, P. J., Quezada, M., Gillespie, S. M., Duveau, D. Y., Michalowski, A. M., Shinn, P., Guha, R., Ferrer, M., Klumpp-Thomas, C., . . . Monje, M. (2019). Therapeutic strategies for diffuse midline glioma from high-throughput combination drug screening. *Sci Transl Med*, *11*(519). https://doi.org/10.1126/scitranslmed.aaw0064.

Liu, R., Shuai, Y., Luo, J., & Zhang, Z. (2019). SEMA3C Promotes Cervical Cancer Growth and Is Associated With Poor Prognosis. *Front Oncol*, *9*, 1035. https://doi.org/10.3389/fonc.2019.01035.

Long, T., Hassan, A., Thompson, B. M., McDonald, J. G., Wang, J., & Li, X. (2019). Structural basis for human sterol isomerase in cholesterol biosynthesis and multidrug recognition. *Nat Commun*, *10*(1), 2452. https://doi.org/10.1038/s41467-019-10279-w.

Mazzio, E. A., & Soliman, K. F. A. (2018). Whole-transcriptomic Profile of SK-MEL-3 Melanoma Cells Treated with the Histone Deacetylase Inhibitor: Trichostatin A. *Cancer Genomics Proteomics*, *15*(5), 349-364. https://doi.org/10.21873/cgp.20094.

Nagaraja, S., Vitanza, N. A., Woo, P. J., Taylor, K. R., Liu, F., Zhang, L., Li, M., Meng, W., Ponnuswami, A., Sun, W., Ma, J., Hulleman, E., Swigut, T., Wysocka, J., Tang, Y., & Monje, M. (2017). Transcriptional Dependencies in Diffuse Intrinsic Pontine Glioma. *Cancer Cell*, *31*(5), 635-652 e636. https://doi.org/10.1016/j.ccell.2017.03.011.

Park, A., & Harris, L. K. (2021). Gene Expression Meta-Analysis Reveals Interferon-Induced Genes Associated With SARS Infection in Lungs. *Front Immunol*, *12*, 694355. https://doi.org/10.3389/fimmu.2021.694355.

Peacock, J. W., Takeuchi, A., Hayashi, N., Liu, L., Tam, K. J., Al Nakouzi, N., Khazamipour, N., Tombe, T., Dejima, T., Lee, K. C., Shiota, M., Thaper, D., Lee, W. C., Hui, D. H., Kuruma, H., Ivanova, L., Yenki, P., Jiao, I. Z., Khosravi, S., . . . Ong, C. J. (2018). SEMA3C drives cancer growth by transactivating multiple receptor tyrosine kinases via Plexin B1. *EMBO Mol Med*, *10*(2), 219-238. https://doi.org/10.15252/emmm.201707689.

Pellot, J. E., & De Jesus, O. (2021). Diffuse Intrinsic Pontine Glioma. *StatPearls [Internet]*.

Rechberger, J. S., Lu, V. M., Zhang, L., Power, E. A., & Daniels, D. J. (2020). Clinical trials for diffuse intrinsic pontine glioma: the current state of affairs. *Childs Nerv Syst*, *36*(1), 39-46. https://doi.org/10.1007/s00381-019-04363-1.

Sahni, J. M., & Keri, R. A. (2018). Targeting bromodomain and extraterminal proteins in breast cancer. *Pharmacol Res*, *129*, 156-176. https://doi.org/10.1016/j.phrs.2017.11.015.

Schinke, C. D., Bird, J. T., Qu, P., Yaccoby, S., Lyzogubov, V. V., Shelton, R., Ling, W., Boyle, E. M., Deshpande, S., Byrum, S. D., Washam, C., Mackintosh, S., Stephens, O., Thanendrarajan, S., Zangari, M., Shaughnessy, J., Jr., Zhan, F., Barlogie, B., van Rhee, F., & Walker, B. A. (2021). PHF19 inhibition as a therapeutic target in multiple myeloma. *Curr Res Transl Med*, *69*(3), 103290. https://doi.org/10.1016/j.retram.2021.103290.

Srikanthan, D., Taccone, M. S., Van Ommeren, R., Ishida, J., Krumholtz, S. L., & Rutka, J. T. (2021). Diffuse intrinsic pontine glioma: current insights and future directions. *Chin Neurosurg J*, *7*(1), 6. https://doi.org/10.1186/s41016-020-00218-w.

Subramanian, A., Tamayo, P., Mootha, V. K., Mukherjee, S., Ebert, B. L., Gillette, M. A., Paulovich, A., Pomeroy, S. L., Golub, T. R., Lander, E. S., & Mesirov, J. P. (2005). Gene set

enrichment analysis: a knowledge-based approach for interpreting genome-wide expression profiles. *Proc Natl Acad Sci U S A*, *102*(43), 15545-15550. https://doi.org/10.1073/pnas.0506580102.

Taylor, I. C., Hutt-Cabezas, M., Brandt, W. D., Kambhampati, M., Nazarian, J., Chang, H. T., Warren, K. E., Eberhart, C. G., & Raabe, E. H. (2015). Disrupting NOTCH Slows Diffuse Intrinsic Pontine Glioma Growth, Enhances Radiation Sensitivity, and Shows Combinatorial Efficacy With Bromodomain Inhibition. *J Neuropathol Exp Neurol*, *74*(8), 778-790. https://doi.org/10.1097/NEN.0000000000000216.

Theodoropoulos, P. C., Wang, W., Budhipramono, A., Thompson, B. M., Madhusudhan, N., Mitsche, M. A., McDonald, J. G., De Brabander, J. K., & Nijhawan, D. (2020). A Medicinal Chemistry-Driven Approach Identified the Sterol Isomerase EBP as the Molecular Target of TASIN Colorectal Cancer Toxins. *J Am Chem Soc*, *142*(13), 6128-6138. https://doi.org/10.1021/jacs.9b13407.

Tu, B., Zhang, M., Liu, T., & Huang, Y. (2020). Nanotechnology-Based Histone Deacetylase Inhibitors for Cancer Therapy. *Front Cell Dev Biol*, *8*, 400. https://doi.org/10.3389/fcell.2020.00400.

Wang, J., Huang, T. Y., Hou, Y., Bartom, E., Lu, X., Shilatifard, A., Yue, F., & Saratsis, A. (2021). Epigenomic landscape and 3D genome structure in pediatric high-grade glioma. *Sci Adv*, *7*(23). https://doi.org/10.1126/sciadv.abg4126.

Wang, L., Tan, T. K., Durbin, A. D., Zimmerman, M. W., Abraham, B. J., Tan, S. H., Ngoc, P. C. T., Weichert-Leahey, N., Akahane, K., Lawton, L. N., Rokita, J. L., Maris, J. M., Young, R. A., Look, A. T., & Sanda, T. (2019). ASCL1 is a MYCN- and LMO1-dependent member of the adrenergic neuroblastoma core regulatory circuitry. *Nat Commun*, *10*(1), 5622. https://doi.org/10.1038/s41467-019-13515-5.

Wang, S. C., Liao, L. M., Ansar, M., Lin, S. Y., Hsu, W. W., Su, C. M., Chung, Y. M., Liu, C. C., Hung, C. S., & Lin, R. K. (2021). Automatic Detection of the Circulating Cell-Free Methylated DNA Pattern of GCM2, ITPRIPL1 and CCDC181 for Detection of Early Breast Cancer and Surgical Treatment Response. *Cancers (Basel)*, *13*(6). https://doi.org/10.3390/cancers13061375.